Body mass index, time of day and genetics affect perivascular spaces in the white matter

Giuseppe Barisano[1,2] ⓘ, Nasim Sheikh-Bahaei[3], Meng Law[1,4,5,6],
Arthur W Toga[1] and Farshid Sepehrband[1]

Abstract

The analysis of cerebral perivascular spaces (PVS) using magnetic resonance imaging (MRI) allows to explore *in vivo* their contributions to neurological disorders. To date the normal amount and distribution of PVS in healthy human brains are not known, thus hampering our ability to define with confidence pathogenic alterations. Furthermore, it is unclear which biological factors can influence the presence and size of PVS on MRI. We performed exploratory data analysis of PVS volume and distribution in a large population of healthy individuals (n = 897, age = 28.8 ± 3.7). Here we describe the global and regional amount of PVS in the white matter, which can be used as a reference for clinicians and researchers investigating PVS and may help the interpretation of the structural changes affecting PVS in pathological states. We found a relatively high inter-subject variability in the PVS amount in this population of healthy adults (range: 1.31–14.49 cm^3). The PVS volume was higher in older and male individuals. Moreover, we identified body mass index, time of day, and genetics as new elements significantly affecting PVS *in vivo* under physiological conditions, offering a valuable foundation to future studies aimed at understanding the physiology of perivascular flow.

Keywords

Perivascular spaces, magnetic resonance imaging, body mass index, time of day, genetics

Introduction

Perivascular spaces (PVS), also known as Virchow-Robin spaces, are tube-shaped structures that surround perforating arteries and small blood vessels in the brain parenchyma, including arterioles, venules, and capillaries.[1] PVS is a major component of the brain clearance system and accommodates the influx of CSF to the cerebral parenchyma through the peri-arterial space and the efflux of interstitial fluid to the lymphatic system through the peri-venous space.[2,3] Detecting pathological PVS changes is of high clinical significance because it provides mechanistic insight into disease pathology, aids in diagnosis, and can be used for disease monitoring, as PVS alterations may precede and be more reversible than demyelination and axonal loss in neurodegenerative disorders.[4,5] However, the physiological profile of the PVS is not fully understood, limiting the ability to identify and recognize PVS

[1]Laboratory of Neuro Imaging, USC Stevens Neuroimaging and Informatics Institute, Keck School of Medicine, University of Southern California, Los Angeles, CA, USA
[2]Neuroscience Graduate Program, University of Southern California, Los Angeles, CA, USA
[3]Department of Radiology, Keck Hospital of USC, Keck School of Medicine, University of Southern California, Los Angeles, CA, USA
[4]Department of Neurological Surgery, Keck Hospital of USC, Keck School of Medicine, University of Southern California, Los Angeles, CA, USA
[5]Department of Neuroscience, Monash University, Melbourne, Australia
[6]Department of Radiology, Alfred Health, Monash University, Melbourne, Australia

Corresponding author:
Giuseppe Barisano, Laboratory of Neuro Imaging, Stevens Neuroimaging and Informatics Institute, Keck School of Medicine, University of Southern California, 2025 Zonal Avenue, Los Angeles, CA 90033, USA.
Email: giuseppe.barisano@loni.usc.edu

abnormalities in neurological disorders, especially in subclinical phases of the disease.

In the past two decades, improvements in imaging and post-processing techniques as well as the more widespread use of ultra-high field MRI systems supported significantly enhanced evaluation of PVS, and increasing attention has been dedicated to PVS, their pathophysiological variations, and their potential role as a diagnostic biomarker.[6–9] In fact, to date increased PVS visibility on human MRI studies has been found associated with aging[10] and a number of pathologic conditions, such as neuropsychiatric and sleep disorders,[11–15] multiple sclerosis,[16,17] mild traumatic brain injury,[18,19] Parkinson's disease,[20] post-traumatic epilepsy,[19] myotonic dystrophy,[21] systemic lupus erythematosus,[22] cerebral small vessel disease,[23–27] and cerebral amyloid-β pathologies, including Alzheimer's disease and cerebral amyloid angiopathy.[28–31] These findings suggest that a higher number of MRI-visible PVS might be an indicator of impaired brain health, although not specific for any single disease.

Despite the increased interest in the role of PVS within the scientific community, there are several unsolved controversies regarding *in vivo* PVS analysis using MRI. Resolving these issues is critical for the interpretation of the results derived from PVS studies.[5,32] Some of the main problems include: 1) the definition of the enlarged PVS: traditionally, the increased number of detected PVS on MRI has been interpreted as an enlargement of PVS, but there is no agreement regarding the radiological definition of enlarged PVS, as there is no quantitative measure of PVS in healthy people; 2) the visual scoring used in most studies focus on basal ganglia and centrum semiovale, but the distribution of PVS in other regions of the white matter is unknown; 3) the role and effect of clinical and genetic factors on the physiological amount of PVS have not been thoroughly investigated.

In this study, we provide the first quantitative analysis of PVS performed using submilliter MRI in a large population of 897 healthy adults from the human connectome project (HCP).[33] We describe the regional distribution and extent of PVS in the white matter of the human brain, which can be used by researchers and clinicians as a resource for the quantitative analysis of physiological PVS. The age range of participants was 22–37 years old and was chosen to represent healthy adults beyond the age of major neurodevelopmental changes and before the onset of neurodegenerative alterations.[33] We also investigated the relationship between PVS and multiple demographic, clinical, and genetic parameters in order to understand which factors may significantly influence the amount of PVS in healthy adults.

Material and methods

Study population

A total of 897 participants were identified from the HCP study (S900 release).[33] According to how the HCP study has been designed and performed, recruiting efforts were aimed at ensuring that participants broadly reflect the ethnic and racial composition of the U.S. population as represented in the 2000 decennial census.[34] The goal was to recruit a pool of individuals that is generally representative of the population at large, in order to capture a wide range of variability in healthy individuals with respect to behavioral, ethnic, and socioeconomic diversity.[34] The study protocol was approved by the Institutional Review Board at the University of Southern California (IRB# HS-19-00448) conforming with the World Medical Association Declaration of Helsinki. Written consent was obtained from all participants at the beginning of the first day of involvement in the project.[34] Only healthy individuals were included in the study (inclusion and exclusion criteria listed in Supplementary Table 1).

Clinical and behavioral data

Collected demographic and clinical data included: age, sex, height and weight with the corresponding body mass index (BMI), blood pressure, years of education, hematocrit, glycated hemoglobin, and thyroid-stimulating hormone in blood. Information about alcohol consumption and tobacco smoking was collected through the Semi-Structured Assessment for the Genetics of Alcoholism interview (SSAGA).[35] The NIH Toolbox (http://www.nihtoolbox.org) was used to assess the domains of cognition, emotion, motor function, and sensation.[33] Additionally, each participant underwent the Mini-Mental State Examination (MMSE).[36] The Pittsburgh Sleep Quality Index was used to evaluate sleep quality and quantity[37] (Supplementary Material).

MRI methods and analysis

The preprocessed T1-weighted (TR 2400 ms, TE 2.14 ms, TI 1000 ms, FOV 224x224 mm) and T2-weighted (TR 3200 ms, TE 5.65 ms, FOV 224x224 mm) images of the HCP,[38] acquired at 0.7 mm³ resolution on a Siemens 3T Skyra scanner (Siemens Medical Solutions, Erlangen, Germany), were used for the PVS analysis. Multiple quality control steps have been applied before, during, and after each scan session, in order to acquire high quality MRI data with minimal occurrence of motion artifacts.[39] The preprocessing steps included: correction for gradient

nonlinearity, readout, and bias field; alignment to anterior commissure-posterior commissure subject space; registration to MNI 152 space using the FNIRT function in FSL;[40] generation of individual cortical, white matter, and pial surfaces and volumes using the FreeSurfer software[41] and the HCP pipelines.[38]

PVS analysis

For PVS quantification and mapping, we first enhanced the visibility of PVS and then automatically segmented PVS across the white matter. We combined T1- and T2-weighted images that were adaptively filtered to remove non-structured high-frequency spatial noise by using a filtering patch which removes the noise at a single-voxel level and preserves signal intensities that are spatially repeated, thus preserving PVS voxels.[42,43] Non-local mean was used for removing high frequency noise, which measures the image intensity similarities by considering the neighboring voxels in a blockwise fashion, where filtered image is $\sum_{x_i \in V_i} \omega(x_i, x_j) u(x_j)$. For each voxel (x_j) the weight (ω) is measured using the Euclidean distance between 3D patches. The adaptive non-local mean filtering technique adds a regularization term to the above formulation to remove bias intensity of the Rician noise observed in MRI.

We then used n-tissue parcellation technique of the Advanced Normalization Tools (ANTs) package.[44,45] Parcellated white matter was used as a mask for PVS analysis. For PVS segmentation, we first applied Frangi filter,[46] using Quantitative Imaging Toolkit,[47] which extracts the likelihood of a voxel belonging to a PVS. The Frangi filter has been shown to be an adequate tool for PVS segmentation.[42,48–52] Frangi filter estimates a vesselness measure for each voxel from eigenvectors of the Hessian matrix of the image. Default parameters of $\alpha = 0.5$, $\beta = 0.5$ and c were used, as recommended in Ref.46 The parameter c was set to half the value of the maximum Hessian norm. Frangi filter estimated vesselness measures at different scales and provided the maximum likeliness. The scale was set to a large range of 0.1–5 voxels in order to maximize the vessel inclusion. The output of this step is a quantitative maximum likelihood map of vessels in regions of interest (ROIs).[46] We selected a previously optimized scaled threshold of 1.5 (equal to raw threshold of 1e–6) in the vessel map in order to obtain a binary mask of PVS regions, which is required for obtaining PVS volumetric measurements and spatial distribution.[42]

The periventricular voxels were excluded via a dilated mask of the lateral ventricles in order to remove the incorrectly segmented PVS at the lateral ventricles-white matter boundary.[42] This PVS segmentation technique has been previously validated on the same MRI dataset.[42] Two expert PVS readers independently counted the PVS in the centrum semiovale of 100 MRI scans according to a validated visual rating scale.[53] The number of PVS obtained with our segmentation algorithm was compared with the numbers obtained by the experts: Lin's concordance coefficient between the automated and the experts' PVS counts was 0.81, the bias correction value was 0.88, and the Pearson correlation coefficient was 0.61.[42]

Furthermore, the expert PVS readers reviewed 30 additional PVS masks and manually edited them removing the false positives PVS and segmenting the false negatives PVS in order to estimate the sensitivity and specificity of our segmentation technique to PVS voxels. The sensitivity and specificity were $97.7 \pm 1.6\%$ and $97.8 \pm 1.8\%$ (mean $\pm$ standard deviation), respectively. Among the 130/897 MRI scans and PVS masks visually analyzed by the expert readers, none of the images presented motion artifacts affecting the PVS segmentation. Finally, PVS ratio was extracted across the white matter regions, parcellated based on Desikan-Killiany atlas using *FreeSurfer* software.[54] The total PVS-white matter ratio was also estimated.

Genome-wide association analysis

The genome-wide association analysis is described in the Supplementary Material.

Statistical analysis

The statistical analysis was done using the R package version 1.2.5.[55]

The Shapiro-Wilk test for normality was used to assess data distribution. All data analyzed exhibited a distribution that was significantly different from normal distribution. Therefore, the following nonparametric tests were applied: the Wilcoxon matched-pairs signed rank test to compare differences across paired groups; the Wilcoxon rank sum (Mann-Whitney) test to compare two unmatched groups; the Kruskal-Wallis test to compare three or more unmatched group; correlations were measured using the Spearman's coefficient.

In order to assess which demographic and clinical parameters influenced the amount of PVS measured in the brain, general linear models were applied, using one clinical factor at a time as independent variable, and the PVS ratio as dependent variable. The following factors were investigated: age, BMI, gender, systolic blood pressure, diastolic blood pressure, thyroid-stimulating hormone level, hematocrit, and glycated hemoglobin. After the identification of potentially significant factors, we performed a new general linear

model analysis including all of them together as independent variables and the PVS ratio as the dependent variable. The two-way ANCOVA model was used to test the effect of gender and BMI on the PVS ratio controlling for age. On a separate analysis, we also investigated whether cigarette smoking and alcohol affect PVS.

When analyzing the relationship between PVS ratio and the results of the behavioral tests, a principal component analysis was initially applied to convert and reduce this set of variables into a set of linearly uncorrelated variables, since many of the behavioral scores were expected to have multi-collinearity. The first principal component, explaining most of the variance in behavioral measures, was then used to identify the most influential neurocognitive scores, which were employed in a series of linear models as dependent variables to investigate whether the PVS ratio is a predictor of cognitive performance. Regression models were fitted using the ordinary least square technique. The Benjamini-Hochberg method was adopted to correct for multiple comparisons with a false discovery rate of 0.05. All p-values were 2-sided and considered significant at <0.05.

Results

Analysis of PVS volume, ratio, and distribution across white matter regions

We were able to compute PVS volume in 897 participants (demographic and clinical data are reported in Table 1).

The mean PVS volume in the white matter was $5.03 \pm 2.15 \, cm^3$, with a high inter-subject variability (median: $4.68 \, cm^3$; 1st quartile ($q_{0.25}$): $3.40 \, cm^3$; 3rd quartile ($q_{0.75}$): $6.21 \, cm^3$; range: $1.31–14.49 \, cm^3$) (Figure 1). The interquartile range (IQR) criterion was used to identify potential outliers: PVS values below $q_{0.25} - 1.5 \times IQR$ or above $q_{0.75} + 1.5 \times IQR$ were considered potential outliers. Based on this criterion, we identified 16/897 cases with total PVS volume in the white matter above $q_{0.75} + 1.5 \times IQR$ (range: $10.88–14.49 \, cm^3$). The corresponding PVS masks were visually analyzed by the expert readers. Since none of the PVS masks presented any major false positive which could explain the high value, we have not excluded them from the subsequent analyses.

Among the ROIs segmented in the white matter, the superior frontal and parietal regions showed the highest percentage of PVS, including on average more than

Table 1. Demographic and clinical characteristics of participants from the Human Connectome Project (S900 Release) included in this study.

	Population		
	Male	Female	Overall
Age	28 ± 3.65	29.46 ± 3.58	28.82 ± 3.68
BMI, kg/m^2 (n = 896)	26.95 ± 4.52	26.42 ± 5.84	26.65 ± 5.3
Education (years)	14.77 ± 1.79	14.98 ± 1.84	14.89 ± 1.82
Mini-mental state examination score (out of 30)	28.96 ± 1.1	29.05 ± 0.96	29.01 ± 1.03
Smoking history (n = 896)			
-Non-smokers	186	304	490
-Occasional smokers	87	89	176
-Regular smokers	121	109	230
Average number of cigarettes/day	10.08 ± 5.66	9.72 ± 6.41	9.91 ± 6.02
Average alcoholic drinks/week (n = 880)	6.47 ± 8.29	3.06 ± 4.34	4.54 ± 6.58
Systolic blood pressure (mmHg) (n = 884)	129.29 ± 13.6	120.13 ± 13.66	124.17 ± 14.36
Diastolic blood pressure (mmHg) (n = 884)	79.11 ± 10.34	75.22 ± 10.38	76.94 ± 10.54
Hematocrit (%) (n = 823)	46.03 ± 3.57	40.87 ± 4.43	43.12 ± 4.81
Blood thyroid hormone (mU/L) (n = 610)	1.73 ± 0.91	1.82 ± 1.31	1.78 ± 1.13
Glycated hemoglobin (%) (n = 603)	5.26 ± 0.41	5.26 ± 0.39	5.26 ± 0.4
Average amount of sleep hours per night	6.81 ± 1.15	6.82 ± 1.14	6.81 ± 1.15
Neuroimaging data			
Total intracranial volume (cm^3)	1702.86 ± 148.21	1470.94 ± 149.79	1572.81 ± 188.33
Whole brain volume (cm^3)	1264.98 ± 103.12	1106.78 ± 85.79	1176.28 ± 122.31
White matter volume (cm^3)	480.28 ± 50.41	415.27 ± 40.70	443.83 ± 55.54
PVS volume (mm^3)	5842.93 ± 2356.69	4393.76 ± 1733.64	5029.39 ± 2153.15
PVS ratio (%)	1.22 ± 0.45	1.07 ± 0.39	1.14 ± 0.43

N=897 unless otherwise specified. Data are mean ± standard deviation.
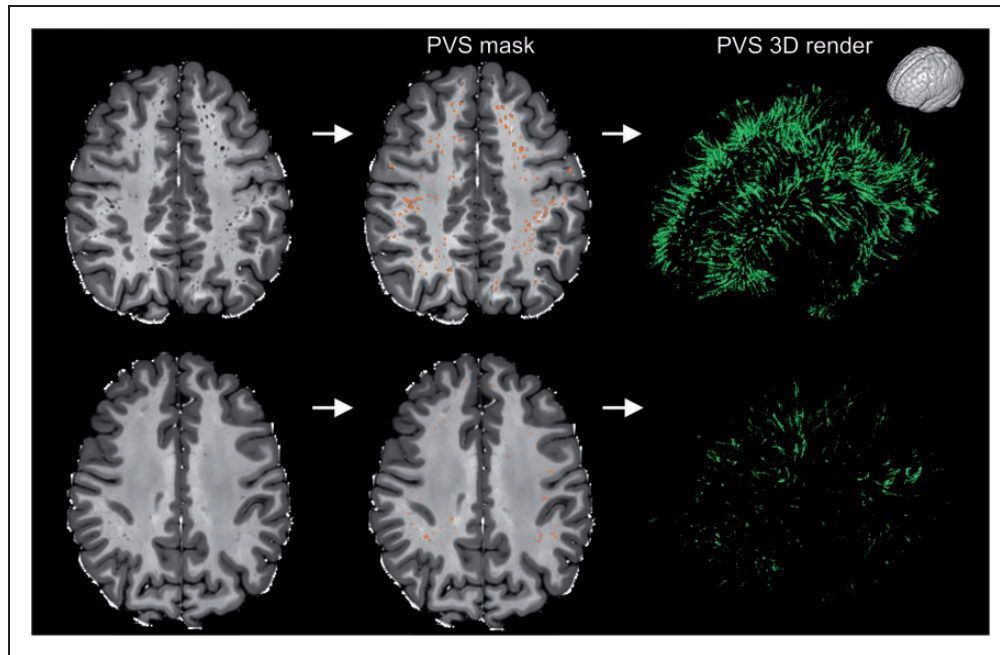
Figure 1. Examples showing the high inter-subject variability of perivascular spaces (PVS) in healthy participants. The participant on the top is a 32 years old male, while the participant on the bottom is a 22 years old female (two extreme cases are intentionally presented to highlight the high inter-subject variability in PVS). The MRI scans are shown on the left column and the PVS mask were overlaid in the center (orange). The images on the right are the corresponding 3D maps of the PVS masks. The orientation of the 3D maps is reported on the top right corner.

8% and 6% of the total PVS volume, respectively (Figure 2(a) and Supplementary Figure 1).

We observed a significant relationship between the PVS volume and the measured white matter volume, as assumed *a priori* ($r = 0.52$, $p < 0.0001$) (Figure 2(b)). Therefore, we calculated the PVS ratio, corresponding to the ratio between the PVS volume and the white matter volume.

The average PVS ratio in the whole white matter was $1.14 \pm 0.43\%$ (range: 0.34-3.13%). The regions with the highest PVS ratios were the white matter areas adjacent to the cingulate cortex, insula, and supramarginal gyrus (above 3%); on the other hand, the regions with the smallest PVS ratios were the white matter areas underlying the cuneus, entorhinal cortex, and the frontal pole cortex (Figure 2(c), Supplementary Figure 1, and Supplementary Table 2).

When comparing one side of each ROI with its contralateral part in the same subject, the relative difference in PVS ratio was 18% on average, variably exhibiting more PVS on the right or on the left side. All the regions showed a significant asymmetric distribution of PVS (Wilcoxon matched-pairs, $p < 0.01$), except the white matter areas underlying the frontal pole, pars orbitalis and opercularis, anterior cingulate, precentral, transverse temporal, cuneus, and pericalcarine regions. The white matter regions showing on average the highest asymmetric distribution of PVS were

those underlying the lingual gyrus (50% higher PVS ratio on the right side) and the entorhinal cortex (120% higher PVS ratio on the left hemisphere) (Figure 2(d) and Supplementary Table 2).

Together, these results show that an asymmetric distribution of PVS across the two cerebral hemispheres can be considered physiological in most of the ROIs of healthy adults. Additionally, the entity of the asymmetry can be of great extent in some ROIs, with one side having a PVS ratio up to 120% higher than the contralateral side.

The PVS ratio is influenced by body mass index, age, and gender

Next, we investigated which demographic and clinical factors affect the amount of PVS in the brain under physiological conditions. In 897 participants (503 females and 394 males) included in the analysis, the mean age was 29.5 in females and 28 in males. The mean BMI was 26.7 kg/m^2 and was slightly higher in males (26.95) compared with females (26.42). The univariate general linear models testing the clinical factors potentially related with the PVS ratio revealed 4 statistically significant variables: age, BMI, gender and systolic blood pressure ($p < 0.01$ in all cases; Table 2 and Figure 3(a) to (c)). Diastolic blood pressure, thyroid-stimulating hormone level, hematocrit, and glycated
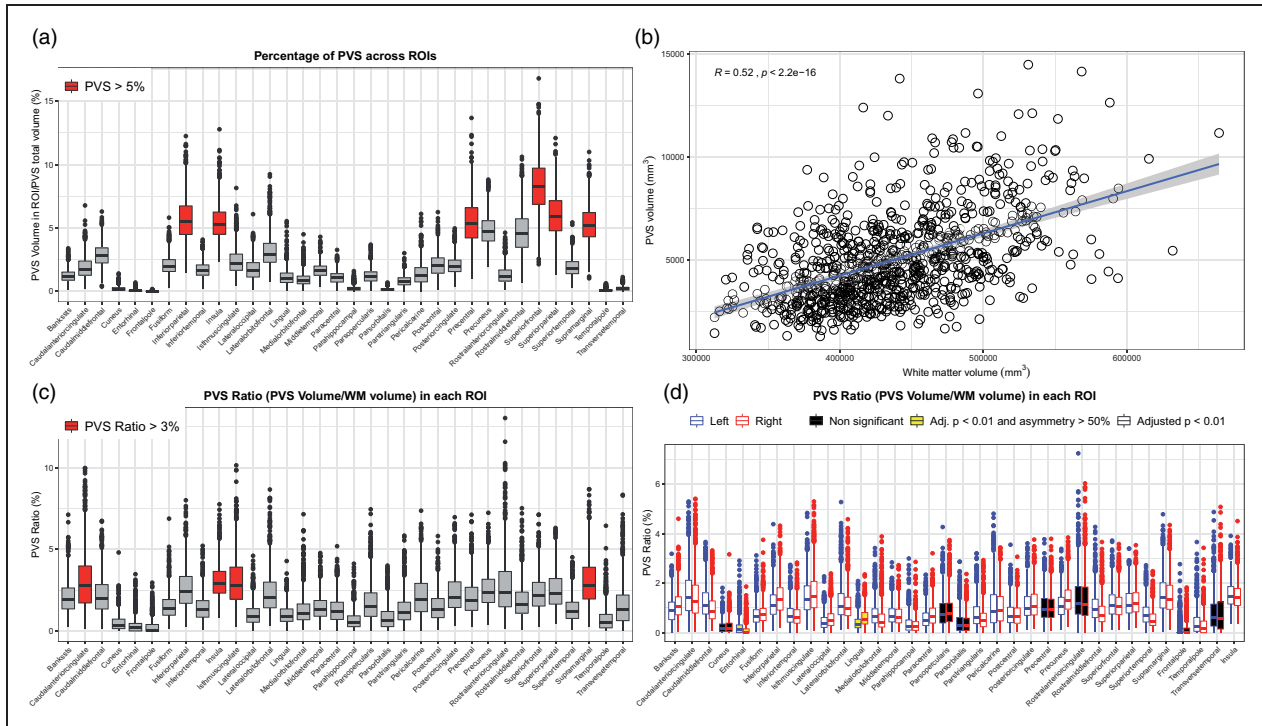
Figure 2. Distribution of the perivascular spaces (PVS) in the white matter and relationship between PVS and white matter. (a) Boxplot showing the percentage of perivascular space (PVS) in each region of interest (ROI). The ROIs showing more than 5% of total PVS volume are highlighted in red. X-axis labels are white matter regions, parcellated based on Desikan-Killiany atlas using *FreeSurfer* software. "Bankssts": Banks of the Superior Temporal Sulcus. (b) Scatterplot showing the significant positive relationship between the measured perivascular space (PVS) and white matter volumes. Spearman's rank correlation coefficient. (c) Boxplot showing the PVS ratio (i.e., PVS volume/white matter volume) in each bilateral region of interest (ROI). The reported value in each ROI is the PVS ratio measured on the right and left side of the specific ROI combined. The ROIs with a PVS ratio higher than 3% are highlighted in red. (d) Boxplot showing the PVS ratio in each unilateral region of interest (ROI). For each ROI, the left boxplot represents the corresponding ROI on the left hemisphere (blue line), while the right boxplot is the corresponding ROI on the right hemisphere (red line). The adjusted p-values refer to the Wilcoxon matched-pairs signed rank test performed in each ROI to compare the two sides. The ROIs with a significant asymmetric distribution of PVS are in white boxes; the ROIs with a significantly asymmetric distribution of PVS having 50% higher PVS ratio on one side compared with its contralateral part are in yellow boxes; the ROIs with a symmetric distribution of PVS ratio across the two hemispheres (i.e., adjusted p-value > 0.01) are in black boxes. Outliers in boxplots show PVS values below $q_{0.25} - 1.5 \times IQR$ or above $q_{0.75} + 1.5 \times IQR$ (panels a, b, and d).

hemoglobin were not significant (Table 2). We included the significant factors as independent variables in a multivariate model testing PVS ratio as dependent variable: higher BMI, older age, and male gender, but not systolic blood pressure, are significant predictors of higher amount of PVS, although the average effect of these factors to PVS is relatively low (Table 2). To further analyze the effects of gender and BMI on PVS, we used a two-way ANCOVA model with 4 BMI groups (< 20, 20–25, 25–30, > 30), adjusting for age. The two-way interaction term between gender and BMI did not reach the statistical significance after controlling for the false discovery rate (Supplementary Table 3, $p = 0.045$). However, on the main effect analyses, we noted that the difference in PVS ratio between males and females is statistically significant in participants with BMI higher than 20 (Figure 3(d)).

Interestingly, while in males the relationship between the increase in PVS ratio and the increase in BMI follows a linear trend, in females the increase in PVS is noted exclusively when the BMI is > 30 (obese people) (Figure 3(d)). This result suggests that the relationship between BMI and PVS is distinct in males and females and not solely determined by a difference in BMI in the two groups.

We also investigated the role that cigarette smoking and alcohol could play in modulating PVS. The PVS ratio was not significantly different in regular smokers, occasional smokers, and non-smokers (Kruskal-Wallis, $p = 0.49$), and the number of cigarettes per day did not significantly correlate with the PVS ratio ($r = -0.04$, $p = 0.55$). The total number of alcoholic drinks consumed in one week on average was not significantly correlated with the PVS ratio ($r = 0.55$, $p = 0.1$).

Table 2. Univariate and multivariate general linear models results.

	Estimate	Confidence interval (95%)	p-value
Series of univariate general linear models with PVS ratio as dependent variable			
Age	0.0162	0.008–0.023	7.18E−05*
BMI	0.0218	0.017–0.027	1.46E−15*
Gender (male)	0.1571	0.102–0.213	1.35E−07*
Diastolic blood pressure	0.0026	−0.00008–0.0053	0.0914
Systolic blood pressure	0.0039	0.002–0.006	0.0002*
Hematocrit	0.0031	−0.003–0.009	0.4204
Thyroid hormone	−0.0012	−0.031–0.028	0.9348
HbA1C	0.0388	−0.046–0.123	0.4204
Multivariate general linear model with PVS ratio as dependent variable			
Age	0.0206	0.010–0.025	7.18E−05*
BMI	0.0176	0.015–0.026	1.46E−15*
Gender (male)	0.1787	0.121–0.236	1.35E−07*
Systolic blood pressure	−0.0009	−0.003–0.001	0.0914
Multivariate general linear model with age-adjusted "cognitive function composite score" as dependent variable			
Gender (male)	5.6255	3.200–8.051	6.06E−06*
Education	5.0297	4.369–5.691	<2E−16*
BMI	−0.4131	−0.648–0.178	0.000597*
PVS ratio	−1.7726	−4.703 − 1.158	0.235489
Multivariate general linear model with age-adjusted "early childhood cognitive score" as dependent variable			
Gender (male)	2.41763	0.404–4.431	0.01864*
Education	3.12245	2.573–3.672	<2E−16*
BMI	−0.29904	−0.495 − 0.104	0.00277*
PVS ratio	−1.95181	−4.382–0.478	0.11527

Significant p-values after controlling for the false discovery rate are marked with *.

In summary, this analysis shows that age, gender, and BMI influence the total volume of PVS, and that the relationship between BMI and PVS is different in males versus females.

## Cognitive functions in healthy adults are not influenced by PVS

Whether the occurrence of MRI-visible PVS in the general elderly population is associated with cognitive dysfunction remains unclear.[56,57] We analyzed the effect of the PVS ratio to cognition in healthy young adults. The average years of education in this population are 14.9 ± 1.8 (range: 11–17) and the mean MMSE is 29 ± 1 (range: 23–30); the education level is slightly higher in females (14.98) compared with males (14.77), and MMSE is not significantly different in females compared with males (29.05 and 28.96, respectively; Wilcoxon, $p = 0.44$). The PVS ratio is not significantly correlated with the level of education ($r = -0.04$, $p = 0.24$, Supplementary Figure 3B) and the MMSE ($r = 0.01$, $p = 0.73$).

We performed a principal component analysis on a set of 19 NIH Toolbox age-adjusted behavioral tests to identify the tests explaining most of the variance: within the first component, explaining 30% of the variance, the most influential tests (loadings > 0.35) are the Cognitive Function Composite score (loading: 0.40)

and the Early Childhood Composite score (loading: 0.37). These age-adjusted scores were included in a linear model (each at a time), corrected by gender and education, as dependent variables to investigate whether the PVS ratio affects cognitive performance. The models showed a significant trend towards the PVS ratio as a factor affecting both the Cognitive Function and the Early Childhood Composite scores ($p = 0.0321$ and $p = 0.0150$, respectively). However, when BMI was added as a covariate in both models, PVS ratio did not reach the statistical significance, while the BMI was found to be a significant factor for both the analyzed cognitive scores ($p < 0.01$ in both cases), where a higher BMI was associated with lower scores (Table 2). These results suggest that a higher amount of PVS in the brain of young adults does not significantly affect cognition, and that higher BMI is associated with lower cognitive scores. Therefore, the apparent association between the greater amount of PVS and worse cognitive performance in a healthy young population is potentially caused by the linear relationship between BMI and PVS.

The PVS ratio is influenced by the time of day

Next, we investigated whether the sleep quality and quantity as well as the time of day play a role in the extent of PVS detectable on MRI. In the whole cohort
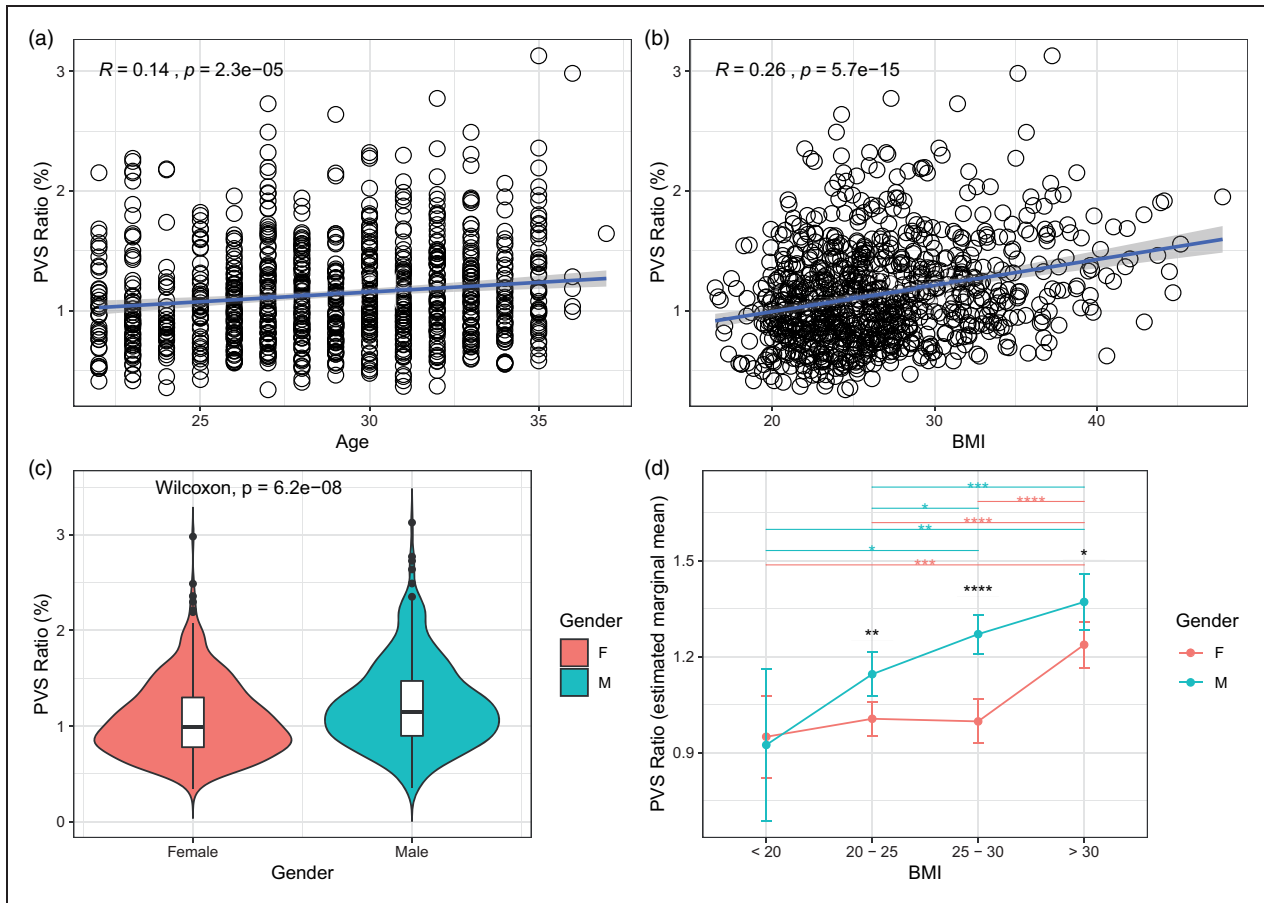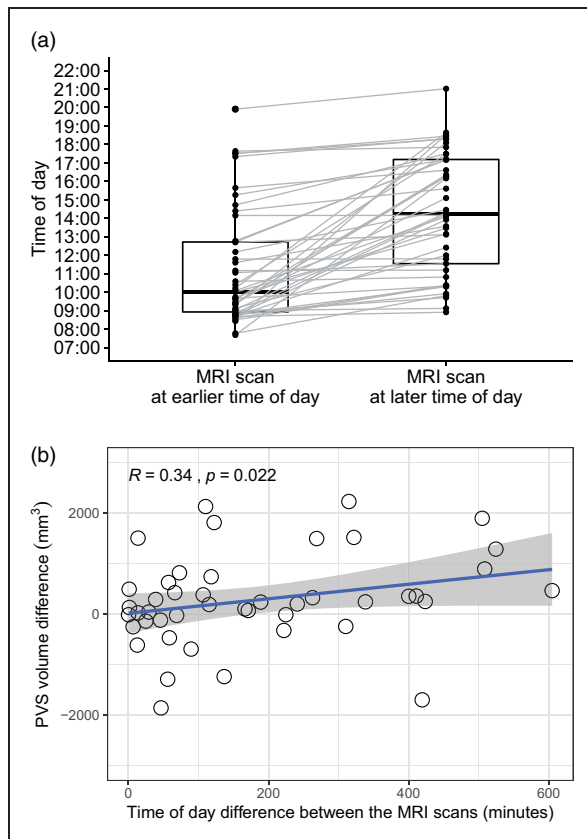
Figure 3. The perivascular space (PVS) ratio is influenced by age, body mass index (BMI), and gender. Scatterplots showing the relationship between PVS and age (a) and BMI (b) (Spearman's rank correlation coefficient). (c) Violin plot showing the statistically significant difference in PVS ratio between males (green) and female (red) participants (Wilcoxon rank sum test). (d) Estimated marginal means of PVS ratio in males and females represented in each BMI group. Significance by ANCOVA for main effects (black *) and post-hoc comparisons (green and red *) controlling for age. The error bars are lower and upper bounds on a 95% confidence interval of the estimate. *: adjusted p-value < 0.05; **: adjusted p-value < 0.01; ***: adjusted p-value $< 1 \times 10^{-3}$; ****: adjusted p-value $< 1 \times 10^{-4}$. The following post-hoc comparisons were not significant after controlling for the false discovery rate: PVS ratio difference in males between BMI groups "20-25" and "25-30"; PVS ratio difference in males between BMI groups "< 20" and "25-30".

($n = 897$), we did not find a significant relationship between PVS ratio and the average number of hours of sleep ($r = -0.05$, $p = 0.11$) or the sleep quality index ($r = 0.04$, $p = 0.2$). 45 participants (31 females, 14 males, mean age: 30.3 ± 3.3) from the HCP S900 release underwent a second MRI scan, with the same scanner and protocol, after 134 ± 63 days (median: 132; $q_{0.25}$: 94; $q_{0.75}$: 154; range: 18–328). We analyzed these scans in order to investigate whether the time of day influences the PVS volume. We tested whether in this dataset the designation of the time of day for the first and second MRI scans could be considered random or not. Based on the time of the earliest and the latest scan (acquired at 7:41 AM and 9:01 PM, respectively), we supposed that the MRI scanner was available from 7:30 AM to 9:30 PM. We assumed time slots of 30

minutes and an equal probability of being scanned in one of the possible 28 slots (from 7:30 AM to 9:00 PM), i.e. 0.04. Therefore, the expected number of participants ($n = 45$) being scanned in each time slot is 1.61 per time slot. For both the first and the second MRI scan, the observed frequency of acquisition times (rounded to the nearest half hour) was not significantly different from the expected (random) frequency of acquisition times (Chi-square test at 1% level of significance, 27 degrees of freedom, $p = 0.78$ and $p = 0.68$, respectively), hence we considered the designation of the time of day for the MRI scans to be random.

The mean BMI (26.9 ± 5.8) and amount of sleep (7.1 ± 0.9 hours) before the first MRI scan were not significantly different from those before the second MRI session (26.6 ± 5.7 and 7.2 ± 0.9, $p = 0.23$ and

Figure 4. The perivascular space (PVS) volume in the single individual changes throughout the day. (a) Boxplot showing the difference in time of day between the MRI scan performed at a later time of day (right) and the MRI scan performed at an earlier time of day (left) in each participant (n=45). (b) Scatterplot showing the relationship between the difference in time-of-day the two MRI scans have been performed (in minutes) and the corresponding changes measured in the perivascular space volume (PVS). Spearman's rank correlation coefficient. None of the values included in this plot is a significant outlier (Extreme studentized deviate method, $p>0.01$).

0.41, respectively). The difference in minutes between the MRI scan performed at a later time of day and the MRI scan performed at an earlier time of day was computed (Figure 4(a)). The intra-individual difference in PVS volume between the MRI scan performed at a later time of day and the MRI scan performed at an earlier time of day was computed. We found a statistically significant relationship between the time difference and the PVS volume change ($r = 0.34$, $p = 0.022$, Figure 4(b)): the increase in PVS volume was greater when the difference between the time-of-day of the two MRI scans was larger. These results suggest that, in people with stable sleep habits, the amount of fluid within the PVS physiologically changes throughout the day, with more fluid detectable at later times of the day.
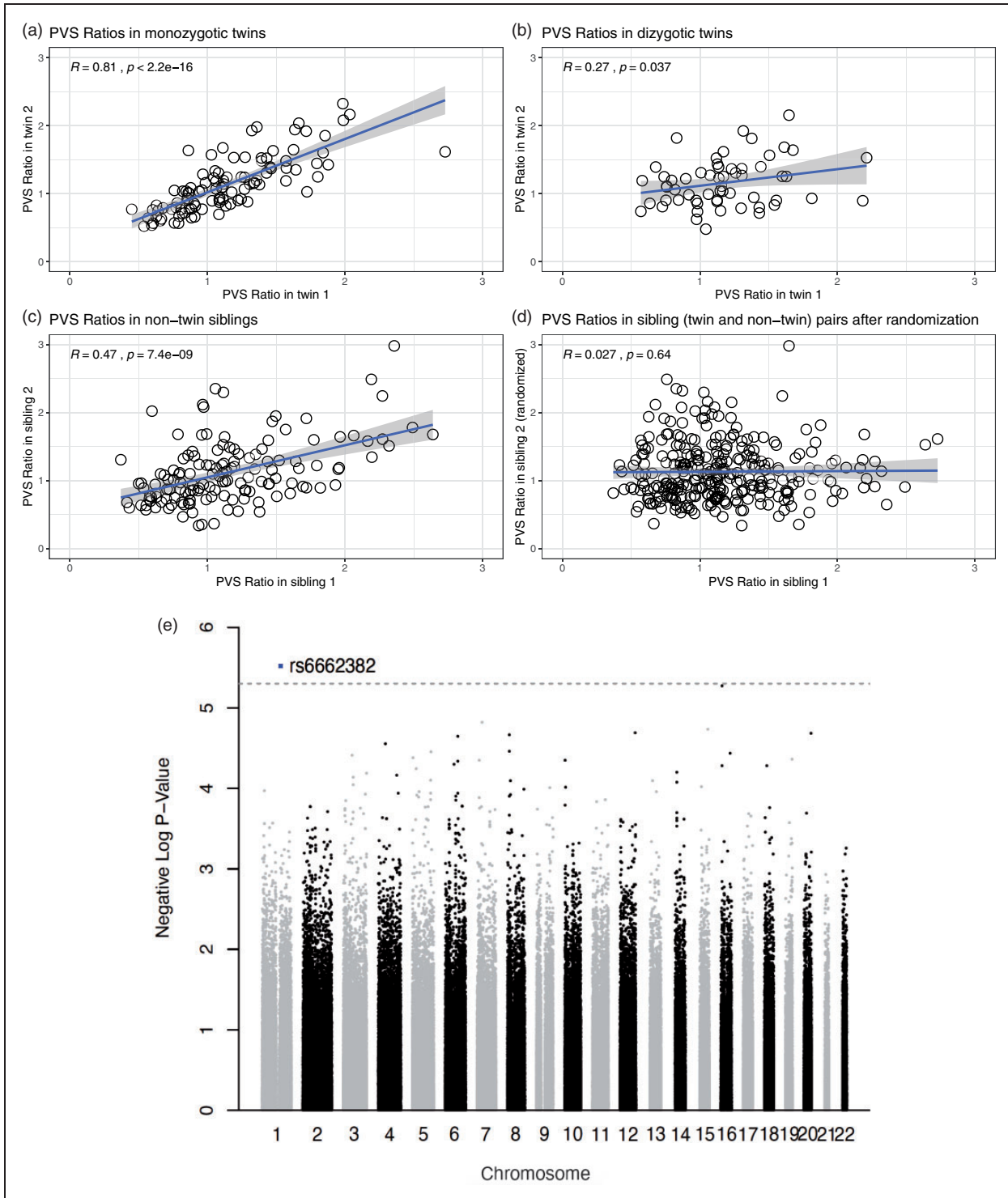
The PVS ratio is influenced by genetic factors

Finally, to study the relationship between PVS and genetic factors, we focused on 3 groups: 51 couples of monozygotic twins (62 females and 40 males, mean age: 29.3 ± 3.4), 29 couples of dizygotic twins (36 females and 22 males, mean age: 29.3 ± 3.3), and 143 couples of non-twin siblings (148 females and 138 males, mean age: 28.4 ± 3.9) available on the HCP dataset. The correlation between the PVS ratio of each participant with the PVS ratio of the corresponding sibling was statistically significant in monozygotic twins and non-twin siblings ($p < 0.01$ in both cases, Figure 5(a) and (c)), but did not reach statistical significance in dizygotic twins after controlling for the false discovery rate, possibly due to the lower sample size ($p = 0.037$, Figure 5 (b)). The correlation was still significant when all couples of siblings (twins and non-twins) were grouped together ($r = 0.54$, $p < 0.01$). After randomization of the pairs, achieved by exchanging one member of the siblings with another member from a different couple, the correlation between the 2 PVS ratios in the new randomized couples was not significant anymore ($r = 0.027$, $p = 0.64$, Figure 5(d)). In any of the 3 groups, the difference in the PVS ratio measured across matched siblings was not correlated with the corresponding difference in BMI between each member of the pairs ($p = 0.91$, 0.34, and 0.97, in monozygotic, dizygotic, and non-twin siblings, respectively, Supplementary Figure 2). These results suggest that genetic factors influence the amount of PVS in the brain.

To gain insights on the specific genetic elements that could affect PVS, we performed a genome-wide association analysis in the 831 participants for which genetic data was available, with the goal of finding single nucleotide polymorphisms (SNPs) associated with PVS ratio. A SNP located in the OR10T2 gene (Olfactory Receptor Family 10 Subfamily T Member 2) in chromosome 1 was found to be significantly associated with PVS ratio at a suggestive association threshold (p = 3E-6. Figure 5(e)).

Discussion

Our findings demonstrate that perivascular spaces display a significant inter-subject variability in a healthy young population and that several factors contribute to the amount of PVS measured on MRI. We confirmed that the absolute volume of PVS is strongly correlated with the white matter volume, corroborating the importance of computing a white-matter-adjusted measure of PVS (PVS ratio). This is usually impracticable in the analysis performed with visual rating scales,

Figure 5. The perivascular space (PVS) ratio is influenced by genetics. Scatterplots showing the relationship of the PVS ratio in each member of the couples plotted against the PVS ratio of the corresponding sibling, in monozygotic twins (a), dizygotic twins (b), and non-twin siblings (c). (d) The correlation is not significant after randomization of one member in each couple, including twins and non-twin siblings. Spearman's rank correlation coefficient. (e) Manhattan plot showing the association *p*-values between SNPs and PVS ratio across the genome.

representing a significant limiting factor for the correct interpretation of the results they can provide.

Concerning the distribution of PVS in the brain, the centrum semiovale and basal ganglia are typically recognized as the area where most of the PVS are usually visible,[58] but the physiological regional division in the white matter is not known. We showed that the majority of PVS are visible in the white matter below the superior frontal and parietal cortices, while the highest PVS ratio was found in the white matter adjacent to the cingulate and insular cortices (*capsulae extrema* and *externa*). Moreover, an asymmetric distribution of PVS across the two hemispheres was found in our healthy population, with some regions presenting more than 50% times higher PVS ratio on one side compared with the contralateral part. These results suggest that an asymmetric distribution of PVS across the white matter is possibly physiological and not related to pathology. Numerous types of data support the hypothesis that the human brain present asymmetries at multiple levels, including gross anatomy, cytoarchitecture, and functional level.[59,60] The cerebral blood flow and metabolic rate measured using Positron Emission Tomography and ^{15}O-labeled radiotracers, for example, were found to be asymmetric in multiple brain regions of healthy subjects, which was interpreted as a physiological asymmetry,[60] possibly caused by anatomical differences in the distribution of blood vessels and/or by the lateralization of brain functions. Similar asymmetries have also been found on functional MRI studies, based on blood oxygenation level-dependent contrast, in healthy people.[61] On the other hand, recent works in stroke and post-traumatic epilepsy show that the asymmetry in perivascular flow may play a key pathogenetic role in those diseases.[19,62,63] Further studies are required to clarify the significance of the asymmetric distribution of PVS volume in the white matter, to understand for example whether it corresponds to an asymmetric distribution of the blood vessels or to asymmetries in the flow of the perivascular fluid.

To our knowledge, this neuroimaging-based PVS map is the most structurally complete atlas of the human PVS to date and can be used as a resource for future quantitative investigations of PVS.

We also investigated factors potentially affecting PVS in a healthy population.

While aging has already been shown to be associated with more MRI-visible PVS,[64] we confirmed this finding even in a population with a relatively narrow age range (22–37). Interestingly, BMI represents a novel factor influencing the amount of PVS: BMI was the most significant variable correlated with PVS ratio in our population, although the correlation was relatively weak. Previous studies have shown that BMI has a linear relationship with CSF pressure in a population with normal CSF pressure values (8–15 mmHg).[65] Even though it was not possible to measure the CSF pressure in our population, this result suggests that the correlation between PVS and BMI could be a consequence of higher CSF pressure in participants with high BMI.

Additionally, obesity is known to critically affect vascular function, including the vascular contractile response,[66] which is thought to be one of the main factors driving fluid movement through the PVS.[67] Hence, vascular contractility could represent another link between BMI and PVS. Nevertheless, since BMI is a non-specific index which can be equally influenced by lean body mass, fat, and body fluid, the biological mechanisms explaining the relationship between BMI and PVS remain to be investigated.

Another interesting finding is that males showed higher PVS ratio than females. Previous studies using visual rating scores have reported greater prevalence of MRI-visible PVS in men compared with women, both in normal elderly and dementia cohorts.[10,31,68] Intriguingly, we observed an age-corrected gender difference in PVS ratio in all BMI groups except in participants with BMI less than 20 and the effect of BMI on PVS ratio is more pronounced in males compared with females, especially in people with BMI between 20 and 30. BMI is positively correlated with plasma biomarkers of inflammation.[69] The astrocytic response to inflammation has been previously demonstrated to be higher in males compared with females, possibly due to the perinatal testosterone which programs astrocytes for a different response to inflammatory challenges.[70] Therefore, the higher amount of PVS we found in male participants compared with BMI-matched females when BMI is higher than 20 might be related to a more vigorous inflammatory response in males, which can affect the perivascular flow and the size of PVS.[70] It would be interesting for future studies to explore the effects of high-fat diet on the cerebrovasculature and the perivascular flow, comparing males and females, and to verify the potentially different changes in the perivascular flow and whether these changes lead to pathological modifications at the cellular and cognitive levels.

Regarding cognitive function, our results do not substantiate a significant relationship between neuropsychological test scores and PVS ratio in young adults, although there is a trend showing more PVS in people who scored worse in some cognitive tests. Remarkably, this trend is mostly explained by the BMI, which appeared as a critical factor in relation with some cognitive scores, where a higher BMI was associated with lower scores. This finding, however, cannot support a biological causal connection between BMI and specific aspects of cognition. For example, it

should be noted that in our population higher BMI was inversely correlated with the level of education (Supplementary Figure 3). In fact, several other epidemiological and cultural factors, potentially associated with BMI and not included in our analysis, could at least partially affect the scores obtained in the neuropsychological tests administered.

Concerning the analysis of sleep, previous human studies showed that people with impaired sleep efficiency and obstructive sleep apnea present increased PVS visibility, which was indirectly interpreted as PVS dysfunction.[15,71] Higher PVS volumes were correlated with objective polysomnography-derived measures of poor sleep quality.[15] Our findings do not show any significant difference in PVS ratio between people on different hours of sleep. This might be due not only to the high inter-subject variability on PVS related to other factors, but also to different body postures exhibited by each participant during sleep,[72] which were not considered in our study. In fact, animal studies showed that the position assumed during sleep is another critical factor affecting the CSF transport in the PVS.[72] Additionally, influence of sleep problems on the brain has been reported to occur in midlife and older ages,[73,74] so the effects on PVS might still be undetectable in the young population that we analyzed.

On the other hand, our results showed the time-of-day as an important element affecting the PVS volume. Specifically, a subset of people that underwent MRI scans twice in different days at different time showed a significantly higher PVS volume in the afternoon and the evening compared with the PVS volume measured on the same individual' scan acquired at an earlier time of day, which is indicative of a circadian fluctuation in the perivascular flow. However, since the interval time between the two scans is relatively large, we cannot fully exclude that the changes detected in PVS volume might be determined by other factors, including aging. Increased uptake of CSF tracer gadobutrol into the entorhinal cortex overnight has been recently shown in patients with idiopathic normal pressure hydrocephalus and controls,[75,76] suggesting a critical role of natural sleep for glymphatic function, as indicated by studies in rodents.[77] A similar fluctuation has been also demonstrated in diffusivity measures of brain tissue derived from diffusion tensor imaging: mean diffusivity, which is significantly influenced by perivascular spaces as well,[78] was found to systematically increase from morning to afternoon scans.[79] More recently, the perivascular flow was also shown to be under circadian control in mice.[80] Here we further validated these findings, showing an increased amount of fluid within the PVS in the white matter at later time of day in the same person. These changes might be related to circadian oscillations in blood pressure and/or

respiration, two regulators of the perivascular flow,[67,81] or to circadian regulation of the flow by aquaporin-4, a water channel supporting the fluid transport from the PVS to the cerebral parenchyma.[80]

Finally, we analyzed for the first time the influence of genetic factors on the PVS ratio in a healthy population. We found that couples of siblings have more similar PVS ratio compared with couples of non-siblings. The similarity was more pronounced in monozygotic twins and was not explained by the difference in BMI. Subsequently, we looked for genome-wide significant association between SNPs and PVS ratio. Although none of the SNPs passed the Bonferroni threshold for GWAS, possibly because of the relatively small sample size of the analyzed cohort, SNPs that are associated with suggestive significance also provide crucial biological insights, given the polygenic and multifactorial nature of many complex phenotypes such as PVS.[82] Interestingly, the SNP showing the most significant association with PVS ratio was located in the OR10T2 gene, a highly conserved region which encodes for one type of olfactory receptors. Previous studies in humans and mammalians have shown an intimate connection between CSF circulation and olfactory-associated perineural, perivascular, and lymphatic compartments, which represent a significant drainage pathway and access route to the brain.[83–87] Olfactory receptors may therefore represent an important regulator of the inflow and outflow of molecules in the perivascular spaces, consequently affecting the amount of fluid within the PVS.

Of note, since the measure and detectability of perivascular spaces depend on the resolution of the images, acquisition parameters, and the field strength of the MRI system[6] and can be significantly influenced by the presence of motion artifacts, a direct comparison of our results with data acquired at different field strength and/or resolution might be inappropriate. In addition to the quality and type of image, the tool used to segment PVS is another critical variable to take into consideration. Several approaches for PVS segmentation have been developed recently:[9,31,42,50,88] although some of them, including ours, make use of the Frangi filter to segment PVS,[9,42,50] it is important to note that different parameters and settings may lead to different outputs and measures of PVS.

This study represents the largest quantitative analysis of PVS in humans using MRI and the only one performed in healthy young adults. These findings can be used as a resource for clinicians and researchers investigating PVS: we provide PVS volumes, PVS/white matter ratios, and their regional distribution that can be helpful when studying PVS under pathological conditions and when attempting to identify patients with abnormal PVS size, location, and

asymmetry. Moreover, we report several novel factors that significantly contribute to the observed high inter-subject variability of PVS visibility in healthy participants, that should be taken into consideration in future research studies analyzing PVS.

Authors' Contribution

G.B., F.S., N.S.B, M.L. and A.W.T. designed the research study. G.B., F.S., and N.S.B. analyzed and interpreted the data. F.S., N.S.B, M.L. and A.W.T. provided critical reading of the manuscript and G.B. wrote the manuscript. All authors edited and revised the manuscript and approved final submission.

Declaration of conflicting interests

The author(s) declared no potential conflicts of interest with respect to the research, authorship, and/or publication of this article.

ORCID iD

Giuseppe Barisano ![ORCID] https://orcid.org/0000-0001-5598-1369

Supplementary material

Supplemental material for this article is available online.

References

1. Zhang ET, Inman CB and Weller RO. Interrelationships of the pia mater and the perivascular (Virchow-Robin) spaces in the human cerebrum. *J Anat* 1990; 170: 111–23.
2. Rasmussen MK, Mestre H and Nedergaard M. The glymphatic pathway in neurological disorders. *Lancet Neurol* 2018; 17: 1016–1024.
3. Tarasoff-Conway JM, Carare RO, Osorio RS, et al. Clearance systems in the brain—implications for Alzheimer disease. *Nat Rev Neurol* 2015; 11: 457.
4. Wardlaw JM, Valdés Hernández MC and Muñoz-Maniega S. What are white matter hyperintensities made of? Relevance to vascular cognitive impairment. *J Am Heart Assoc* 2015; 4: e001140.
5. Brown R, Benveniste H, Black SE, et al. Understanding the role of the perivascular space in cerebral small vessel disease. *Cardiovasc Res* 2018; 114: 1–9.
6. Barisano G, Sepehrband F, Ma S, et al. Clinical 7T MRI: are we there yet? A review about magnetic resonance imaging at ultra-high field. *Br J Radiol* 2018; 91: 20180492.
7. Wardlaw JM, Benveniste H, Nedergaard M, et al. Perivascular spaces in the brain: anatomy, physiology, and contributions to pathology of brain diseases. *Nat Res*. Epub ahead of print 1 March 2020. DOI: 10.1038/s41582-020-0312-z.
8. Cai K, Tain R, Das S, et al. The feasibility of quantitative MRI of perivascular spaces at 7T. *J Neurosci Methods* 2015; 256: 151–156.
9. Zong X, Park SH, Shen D, et al. Visualization of perivascular spaces in the human brain at 7T: sequence optimization and morphology characterization. *Neuroimage* 2016; 125: 895–902.
10. Zhu YC, Dufouil C, Mazoyer B, et al. Frequency and location of dilated Virchow-Robin spaces in elderly people: a population-based 3D MR imaging study. *Am J Neuroradiol* 2011; 32: 709–713.
11. Maclullich AMJ, Wardlaw JM, Ferguson KJ, et al. Enlarged perivascular spaces are associated with cognitive function in healthy elderly men. *J Neurol Neurosurg Psychiatry* 2004; 75: 1519–1523.
12. Taber KH, Shaw JB, Loveland KA, et al. Accentuated Virchow-Robin spaces in the centrum semiovale in children with autistic disorder. *J Comput Assist Tomogr* 2004; 28: 263–268.
13. Rollins NK, Deline C and Morriss MC. Prevalence and clinical significance of dilated Virchow-Robin spaces in childhood. *Radiology* 1993; 189: 53–57.
14. Patankar TF, Baldwin R, Mitra D, et al. Virchow-Robin space dilatation may predict resistance to antidepressant monotherapy in elderly patients with depression. *J Affect Disord* 2007; 97: 265–270.
15. Berezuk C, Ramirez J, Gao F, et al. Virchow-Robin spaces: correlations with polysomnography-derived sleep parameters. *Sleep* 2015; 38: 853–858.
16. Achiron A and Faibel M. Sandlike appearance of Virchow-Robin spaces in early multiple sclerosis: a novel neuroradiologic marker. *Am J Neuroradiol* 2002; 23: 376–380.
17. Wuerfel J, Haertle M, Waiczies H, et al. Perivascular spaces–MRI marker of inflammatory activity in the brain? *Brain* 2008; 131: 2332–2340.
18. Inglese M, Bomsztyk E, Gonen O, et al. Dilated perivascular spaces: hallmarks of mild traumatic brain injury. *Am J Neuroradiol* 2005; 26: 719–724.
19. Duncan D, Barisano G, Cabeen R, et al. Analytic tools for post-traumatic epileptogenesis biomarker search in multimodal dataset of an animal model and human patients. *Front Neuroinform* 2018; 12: 86.
20. Laitinen LV, Chudy D, Tengvar M, et al. Dilated perivascular spaces in the putamen and pallidum in patients with Parkinson's disease scheduled for pallidotomy: a comparison between MRI findings and clinical symptoms and signs. *Mov Disord* 2000; 15: 1139–1144.

21. Di Costanzo A, Di Salle F, Santoro L, et al. Dilated Virchow-Robin spaces in myotonic dystrophy: frequency, extent and significance. *Eur Neurol* 2001; 46: 131–139.

22. Miyata M, Kakeda S, Iwata S, et al. Enlarged perivascular spaces are associated with the disease activity in systemic lupus erythematosus. *Sci Rep* 2017; 7: 1–10.

23. Potter GM, Doubal FN, Jackson CA, et al. Enlarged perivascular spaces and cerebral small vessel disease. *Int J Stroke* 2015; 10: 376–381.

24. Rouhl RPW, van Oostenbrugge RJ, Knottnerus ILH, et al. Virchow-Robin spaces relate to cerebral small vessel disease severity. *J Neurol* 2008; 255: 692–696.

25. Ohba H, Pearce L, Potter G, et al. Enlarged perivascular spaces in lacunar stroke patients. The secondary prevention of small subcortical stroked (SPS3) trial. *Stroke* 2012; 43: A151.

26. Doubal FN, MacLullich AMJ, Ferguson KJ, et al. Enlarged perivascular spaces on MRI are a feature of cerebral small vessel disease. *Stroke* 2010; 41: 450–454.

27. Wardlaw JM, Smith EE, Biessels GJ, et al. Neuroimaging standards for research into small vessel disease and its contribution to ageing and neurodegeneration. *Lancet Neurol* 2013; 12: 822–838.

28. Charidimou A, Jaunmuktane Z, Baron J-C, et al. White matter perivascular spaces: an MRI marker in pathology-proven cerebral amyloid angiopathy? *Neurology* 2014; 82: 57–62.

29. Martinez-Ramirez S, Pontes-Neto OM, Dumas AP, et al. Topography of dilated perivascular spaces in subjects from a memory clinic cohort. *Neurology* 2013; 80: 1551–1556.

30. Roher AE, Kuo Y-M, Esh C, et al. Cortical and leptomeningeal cerebrovascular amyloid and white matter pathology in Alzheimer's disease. *Mol Med* 2003; 9: 112–22.

31. Ramirez J, Berezuk C, Mcneely AA, et al. Visible Virchow-Robin spaces on magnetic resonance imaging of Alzheimer's disease patients and normal elderly from the sunnybrook dementia study. *J Alzheimer's Dis* 2015; 43: 415–424.

32. Woollam DH, Millen JW. The perivascular spaces of the mammalian central nervous system and their relation to the perineuronal and subarachnoid spaces. *J Anat* 1955; 89: 193–200.

33. Van Essen DC, Ugurbil K, Auerbach E, et al. The Human Connectome Project: a data acquisition perspective. *Neuroimage* 2012; 62: 2222–2231.

34. Van Essen DC, Smith SM, Barch DM, et al. The WU-Minn Human Connectome Project: an overview. *Neuroimage* 2013; 80: 62–79.

35. Hu LS, Baxter LC, Smith KA, et al. Relative cerebral blood volume values to differentiate high-grade glioma recurrence from posttreatment radiation effect: direct correlation between image-guided tissue histopathology and localized dynamic susceptibility-weighted contrast-enhanced perfusio. *Am J Neuroradiol* 2008; 30: 552–558.

36. Folstein MF, Robins LN and Helzer JE. The mini-mental state examination. *Arch Gen Psychiatry* 1983; 40: 812.

37. Buysse DJ, Reynolds CF, Monk TH, et al. The Pittsburgh sleep quality index: a new instrument for psychiatric practice and research. *Psychiatry Res* 1989; 28: 193–213.

38. Glasser MF, Sotiropoulos SN, Wilson JA, et al. The minimal preprocessing pipelines for the Human Connectome Project. *Neuroimage* 2013; 80: 105–24.

39. Marcus DS, Harms MP, Snyder AZ, et al. Human Connectome Project informatics: quality control, database services, and data visualization. *Neuroimage* 2013; 80: 202–219.

40. Jenkinson M, Beckmann CF, Behrens TEJ, et al. Fsl. *Neuroimage* 2012; 62: 782–790.

41. Fischl B. FreeSurfer. *Neuroimage* 2012; 62: 774–781.

42. Sepehrband F, Barisano G, Sheikh-Bahaei N, et al. Image processing approaches to enhance perivascular space visibility and quantification using MRI. *Sci Rep* 2019; 9: 12351.

43. Manjón JV, Coupé P, Martí-Bonmatí L, et al. Adaptive non-local means denoising of MR images with spatially varying noise levels. *J Magn Reson Imaging* 2010; 31: 192–203.

44. Avants BB, Tustison N and Song G. Advanced normalization tools (ANTS). *Insight J* 2009; July-December: 1–35.

45. Avants BB, Tustison NJ, Wu J, et al. An open source multivariate framework for N-tissue segmentation with evaluation on public data. *Neuroinformatics* 2011; 9: 381–400.

46. Frangi AF, Niessen WJ, Vincken KL, et al. Multiscale vessel enhancement filtering. *Med Image Comput Comput Interv Miccai'98 1496* 1998; 1496: 130–137.

47. Cabeen RP, Laidlaw DH and Toga AW. Quantitative imaging toolkit: software for interactive 3D visualization, data exploration, and computational analysis of neuroimaging datasets. In: *Proceedings of the joint annual meeting ISMRM-ESMRMB*. Paris, France, 15-18 June 2018, p. 8882. The International Society for Magnetic Resonance in Medicine.

48. Hou Y, Park SH, Wang Q, et al. Enhancement of perivascular spaces in 7 T MR image using Haar transform of non-local cubes and block-matching filtering. *Sci Rep* 2017; 7: 1–12.

49. Zhang J, Gao Y, Park SH, et al. Structured learning for 3-D perivascular space. 2017; 64: 2803–2812.

50. Ballerini L, Lovreglio R, Valdés Hernández MDC, et al. Perivascular spaces segmentation in brain MRI using optimal 3D filtering. *Sci Rep* 2018; 8: 1–11.

51. del Valdés Hernández MC, Ballerini L, Glatz A, et al. Perivascular spaces in the centrum semiovale at the beginning of the 8th decade of life: effect on cognition and associations with mineral deposition. *Brain Imaging Behav*. Epub ahead of print 2019. DOI: 10.1007/s11682-019-00128-1.

52. Ballerini L, Booth T, Valdés Hernández M del C, et al. Computational quantification of brain perivascular space morphologies: associations with vascular risk factors and white matter hyperintensities. A study in the Lothian Birth Cohort 1936. *NeuroImage Clin* 25. Epub ahead of print 1 January 2020. DOI: 10.1016/j.nicl.2019.102120.

53. Potter GM, Chappell FM, Morris Z, et al. Cerebral peri-vascular spaces visible on magnetic resonance imaging: development of a qualitative rating scale and its observer reliability. *Cerebrovasc Dis* 2015; 39: 224–231.

54. Desikan RS, Ségonne F, Fischl B, et al. An automated labeling system for subdividing the human cerebral cortex on MRI scans into gyral based regions of interest. *Neuroimage* 2006; 31: 968–980.

55. R Development Core Team. *R: A language and environment for statistical computing*. Vienna: R Foundation for Statistical Computing, 2019.

56. Del C Valdes Hernandez M, Piper RJ, Wang X, et al. Towards the automatic computational assessment of enlarged perivascular spaces on brain magnetic resonance images: a systematic review. *J Magn Reson Imaging* 2013; 38: 774–785.

57. Hilal S, Tan CS, Adams HHH, et al. Enlarged perivascular spaces and cognition: a meta-analysis of 5 population-based studies. *Neurology* 2018; 91: e832–e842.

58. Kwee RM and Kwee TC. Virchow-Robin spaces at MR imaging. *RadioGraphics* 2007; 27: 1071–1086.

59. Geschwind N and Galaburda AM. Cerebral lateralization: biological mechanisms, associations, and pathology: II. A hypothesis and a program for research. *Arch Neurol* 1985; 42: 521–552.

60. Perlmutter JS, Powers WJ, Herscovitch P, et al. Regional asymmetries of cerebral blood flow, blood volume, and oxygen utilization and extraction in normal subjects. *J Cereb Blood Flow Metab* 1987; 7: 64–67.

61. Powell HWR, Parker GJM, Alexander DC, et al. Hemispheric asymmetries in language-related pathways: a combined functional MRI and tractography study. *Neuroimage* 2006; 32: 388–399.

62. Mestre H, Du T, Sweeney AM, et al. Cerebrospinal fluid influx drives acute ischemic tissue swelling. *Science (80-)* 2020; 367: eaax7171.

63. Feldman RE, Rutland JW, Fields MC, et al. Quantification of perivascular spaces at 7 T: a potential MRI biomarker for epilepsy. *Seizure* 2018; 54: 11–18.

64. Laveskog A, Wang R, Bronge L, et al. Perivascular spaces in old age: assessment, distribution, and correlation with white matter hyperintensities. *Am J Neuroradiol* 2018; 39: 70–76.

65. Berdahl JP, Fleischman D, Zaydlarova J, et al. Body mass index has a linear relationship with cerebrospinal fluid pressure. *Invest Ophthalmol Visual Sci* 2012; 53: 1422–1427.

66. Stapleton PA, James ME, Goodwill AG, et al. Obesity and vascular dysfunction. *Pathophysiology* 2008; 15: 79–89.

67. Iliff JJ, Wang M, Zeppenfeld DM, et al. Cerebral arterial pulsation drives paravascular CSF-interstitial fluid exchange in the murine brain. *J Neurosci* 2013; 33: 18190–18199.

68. Zhu Y-C, Tzourio C, Soumaré A, et al. Severity of dilated Virchow-Robin spaces is associated with age, blood pressure, and MRI markers of small vessel disease: a population-based study. *Stroke* 2010; 41: 2483–2490.

69. Siervo M, Ruggiero D, Sorice R, et al. Body mass index is directly associated with biomarkers of angiogenesis and inflammation in children and adolescents. *Nutrition* 2012; 28: 262–266.

70. Santos-Galindo M, Acaz-Fonseca E, Bellini MJ, et al. Sex differences in the inflammatory response of primary astrocytes to lipopolysaccharide. *Biol Sex Differ* 2011; 2: 7.

71. Song TJ, Park JH, Choi K, et al. Moderate-to-severe obstructive sleep apnea is associated with cerebral small vessel disease. *Sleep Med* 2017; 30: 36–42.

72. Lee H, Xie L, Yu M, et al. The effect of body posture on brain glymphatic transport. *J Neurosci* 2015; 35: 11034–11044.

73. Jelicic M, Bosma H, Ponds RWHM, et al. Subjective sleep problems in later life as predictors of cognitive decline. Report from the Maastricht Ageing Study (MAAS). *Int J Geriatr Psychiatry* 2002; 17: 73–77.

74. Waller KL, Mortensen EL, Avlund K, et al. Subjective sleep quality and daytime sleepiness in late midlife and their association with age-related changes in cognition. *Sleep Med* 2016; 17: 165–173.

75. Ringstad G, Vatnehol SAS and Eide PK. Glymphatic MRI in idiopathic normal pressure hydrocephalus. *Brain* 2017; 140: 2691–2705.

76. Eide PK and Ringstad G. Delayed clearance of cerebrospinal fluid tracer from entorhinal cortex in idiopathic normal pressure hydrocephalus: a glymphatic magnetic resonance imaging study. *J Cereb Blood Flow Metab* 2019; 39: 1355–1368.

77. Xie L, Kang H, Xu Q, et al. Sleep drives metabolite clearance from the adult brain. *Science (80-)* 2013; 342: 373–377.

78. Sepehrband F, Cabeen RP, Choupan J, et al. Perivascular space fluid contributes to diffusion tensor imaging changes in white matter. *Neuroimage* 2019; 197: 243–254.

79. Thomas C, Sadeghi N, Nayak A, et al. Impact of time-of-day on diffusivity measures of brain tissue derived from diffusion tensor imaging. *Neuroimage* 2018; 173: 25–34.

80. Hablitz LM, Plá V, Giannetto M, et al. Circadian control of brain glymphatic and lymphatic fluid flow. *Nat Commun* 2020; 11: 4411.

81. Dreha-Kulaczewski S, Joseph AA, Merboldt KD, et al. Inspiration is the major regulator of human CSF flow. *J Neurosci* 2015; 35: 2485–2491.

82. Le KTT, Matzaraki V, Netea MG, et al. Functional annotation of genetic loci associated with sepsis prioritizes immune and endothelial cell pathways. *Front Immunol* 10. Epub ahead of print 2019. DOI: 10.3389/fimmu.2019.01949.

83. Erlich SS, McComb JG, Hyman S, et al. Ultrastructural morphology of the olfactory pathway for cerebrospinal fluid drainage in the rabbit. *J Neurosurg* 1986; 64: 466–473.

84. Löwhagen P, Johansson BB, Nordborg C. The nasal route of cerebrospinal fluid drainage in man. A light–microscope study. *Neuropathol Appl Neurobiol* 1994; 20: 543–550.

85. Koh L, Zakharov A, Nagra G, et al. Development of cerebrospinal fluid absorption sites in the pig and rat: connections between the subarachnoid space and lymphatic vessels in the olfactory turbinates. *Anat Embryol (Berl)* 2006; 211: 335–344.

86. Kim HJ, Kim PK, Bae SM, et al. Transforming growth factor-β-induced protein (TGFBIp/β ig-h3) activates platelets and promotes thrombogenesis. *Blood* 2009; 114: 5206–5215.

87. Mestre H, Kostrikov S, Mehta RI, et al. Perivascular spaces, glymphatic dysfunction, and small vessel disease. *Clin Sci* 2017; 131: 2257–2274.

88. Boespflug EL, Schwartz DL, Lahna D, et al. MR imaging–based multimodal autoidentification of perivascular spaces (mMAPS): automated morphologic segmentation of enlarged perivascular spaces at clinical field strength. *Radiology* 2018; 286: 632–642.